Dimensionality and morphology of particle and bubble clusters in turbulent flow

ENRICO CALZAVARINI[1,4], MARTIN KERSCHER[2], DETLEF LOHSE[1,4] AND FEDERICO TOSCHI[3,4]

[1]Physics of Fluids Group, Department of Science and Technology, J.M. Burgers Center for Fluid Dynamics, and Impact-Institute, University of Twente, PO Box 217, 7500 AE Enschede, The Netherlands

[2]Mathematisches Institut, Ludwig-Maximilians-Universität, Theresienstrasse 39, D-80333 München, Germany

[3]IAC-CNR, Istituto per le Applicazioni del Calcolo, Viale del Policlinico 137, I-00161 Roma, Italy and INFN,via Saragat 1, I-44100 Ferrara, Italy

[4]International Collaboration for Turbulence Research

We conduct numerical experiments to investigate the spatial clustering of particles and bubbles in simulations of homogeneous and isotropic turbulence. On varying the Stokes parameter and the densities, striking differences in the clustering of the particles can be observed. To quantify these visual findings we use the Kaplan–Yorke dimension. This local scaling analysis shows a dimension of approximately 1.4 for the light bubble distribution, whereas the distribution of very heavy particles shows a dimension of approximately 2.6. However, clearly different parameter combinations yield the same dimensions. To overcome this degeneracy and to further develop the understanding of clustering, we perform a morphological (geometrical and topological) analysis of the particle distribution. For such an analysis, Minkowski functionals have been successfully employed in cosmology, in order to quantify the global geometry and topology of the large-scale distribution of galaxies. In the context of dispersed multiphase flow, these Minkowski functionals – being morphological order parameters – allow us to discern the filamentary structure of the light particle distribution from the wall-like distribution of heavy particles around empty interconnected tunnels. Movies are available with the online version of the paper.

1. Introduction

Even in homogeneous and isotropic turbulence particles, drops and bubbles (all from now on called 'particles') are not distributed homogeneously, but *cluster*, see Crowe, Troutt & Chung (1996) for a classical review article. The clustering has a strong bearing on such diverse issues such as aerosols and cloud formation (Falkovich, Fouxon & Stepanov 2002; Celani *et al.* 2005; Vaillancourt *et al.* 2002), plankton distribution in the deep ocean (Malkiel *et al.* 2006), and sedimentation and CO_2 deposition in water (Upstill-Goddard 2006). Considerable advances in particle tracking velocimetry (La Porta *et al.* 2001; Hoyer *et al.* 2005; Bourgoin *et al.* 2006; Bewley, Lathrop & Sreenivasan 2006; Ayyalasomayajula *et al.* 2006) and in numerics (Elghobashi & Truesdell 1992, 1993; Wang & Maxey 1993; Boivin, Simonin & Squires 1998; Druzhinin & Elghobashi 2001; Marchioli & Soldati 2002; Mazzitelli,
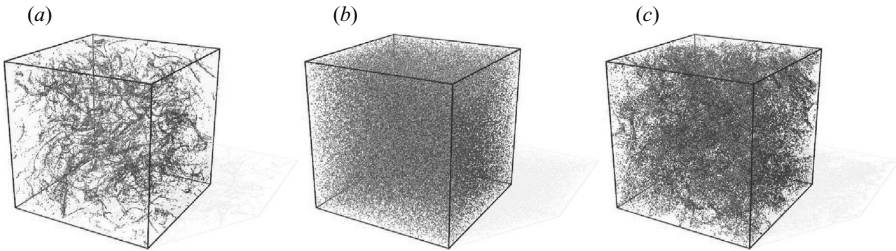
FIGURE 1. Snapshots of the particle distribution in the turbulent flow field for $St = 0.6$ for (a) $\beta = 3$ (bubbles), (b) $\beta = 1$ (tracers), and (c) $\beta = 0$ (heavy particles), all for $Re_\lambda = 75$. Corresponding movies are available with the online version of the paper.

Lohse & Toschi 2003a,b; Biferale *et al.* 2005; Chun *et al.* 2005; van den Berg *et al.* 2006; Bec *et al.* 2006a,b; Calzavarini *et al.* 2007, 2008) now allow the acquisition of huge data sets of particle positions and velocities in turbulence.

In our numerical experiments the fluid flow is simulated by the incompressible Navier–Stokes equation on a 128^3, a 512^3 and a 2048^3 grid with periodic boundary conditions and a large-scale forcing, achieving Taylor–Reynolds numbers of $Re_\lambda = 75$, 180 and 400, respectively. One-way coupled point particles are included which experience inertia forces, added mass forces and drag, i.e. the particle acceleration is given by (Maxey & Riley 1983; Gatignol 1983)

$$\frac{\mathrm{d}\boldsymbol{v}}{\mathrm{d}t} = \beta \frac{\mathrm{D}}{\mathrm{D}t}\boldsymbol{u}(\boldsymbol{x}(t), t) - \frac{1}{\tau_p}(\boldsymbol{v} - \boldsymbol{u}(\boldsymbol{x}(t), t)), \tag{1.1}$$

where $\boldsymbol{v} = \mathrm{d}\boldsymbol{x}/\mathrm{d}t$ is the particle velocity and $\boldsymbol{u}(\boldsymbol{x}(t), t)$ the velocity field. Equation (1.1) holds in the limit of small ($\ll 1$) particle Reynolds number and for particles whose size is small compared to the Kolmogorov length scale η – for finite size particles the results will naturally differ. Lift, buoyancy, two-way coupling and particle–particle interactions are ignored. Besides the Reynolds number the control parameters are the particle radius a, and the density of the fluid ρ_f and of the particle ρ_p. The dimensionless numbers used to characterize the particle in the turbulent flow are the density ratio $\beta = 3\rho_f/(\rho_f + 2\rho_p)$ and the Stokes number $St = \tau_p/\tau_\eta = a^2/(3\beta\eta^2)$, where $\tau_p = a^2/(3\beta\nu)$ is the particle time scale, ν the viscosity, and τ_η the Kolmogorov time scale. In our numerical study we treat β and St as independent parameters. The case $\beta = 0$ (and finite St) corresponds to very heavy particles and $\beta = 3$ to very light particles, e.g. (coated) bubbles (i.e. with no-slip boundary conditions at the interface). $\beta = 1$ means neutral tracers and if in addition $St = 0$ we have fluid particles.

In figure 1 snapshots of the resulting particle distributions from a simulation with $Re_\lambda = 75$, $St = 0.6$ and the total number of particles, $N = 10^5$ are shown. For $\beta = 0$ (heavy particles) and $\beta = 3$ (light bubbles) we observe clustering – but of different type. No clustering is observed for the neutral tracers with $\beta = 1$.

2. Dimensionalities of particle and bubble clusters

How to quantify and characterize the clustering? One way borrowed from dynamical systems theory is to calculate the Kaplan–Yorke dimension D_{KY} in the six-dimensional space spanned by the particle positions and their velocities, see Bec (2003, 2005). The Kaplan–Yorke dimension follows from the Lyapunov exponents (Eckmann & Ruelle 1985), λ_i ($i = 1, \ldots, 6$), and quantifies how contracting the dynamical system is. It is
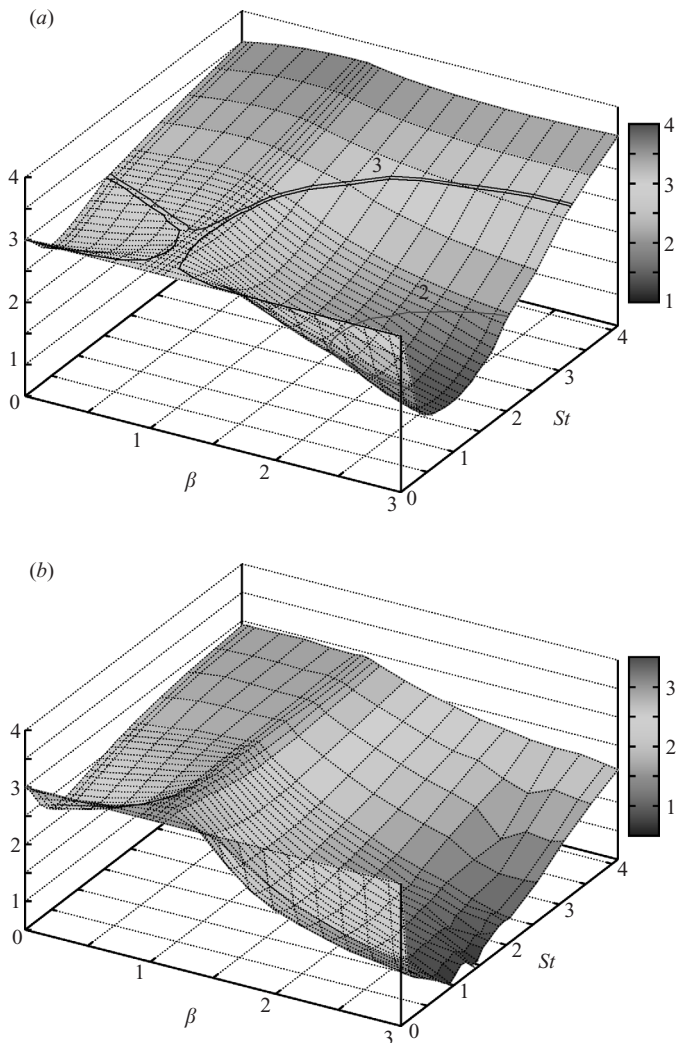
FIGURE 2. (*a*) The Kaplan–Yorke dimension D_{KY} and (*b*) the correlation dimension D_2 of the particle distribution as a function of St and β. The black line in (*a*) marks the value $D_{KY}(\beta, St) = 3$, the grey line the value 2. For the D_{KY} plot 10^6 particles were integrated along the tangent space and for the D_2 plot 5×10^7 particles were followed. In both cases the averaging time was tens of large-eddy turnovers. The particles were grouped in about 500 different types characterized by their (β, St)-values. $Re_\lambda = 75$.

defined as

$$D_{KY} = K + \sum_{i=1}^{K} \lambda_i / |\lambda_{K+1}|,$$

K being the largest integer such that $\sum_{i=1}^{K} \lambda_i \geqslant 0$. Details on the method can be found in Bec (2005), where the case $\beta = 0$ was studied.

In figure 2(*a*) the full landscape of D_{KY} as a function of β and St is shown for $Re_\lambda = 75$; in figure 3 cuts through this landscape for fixed $\beta = 0$, 1, and 3 are
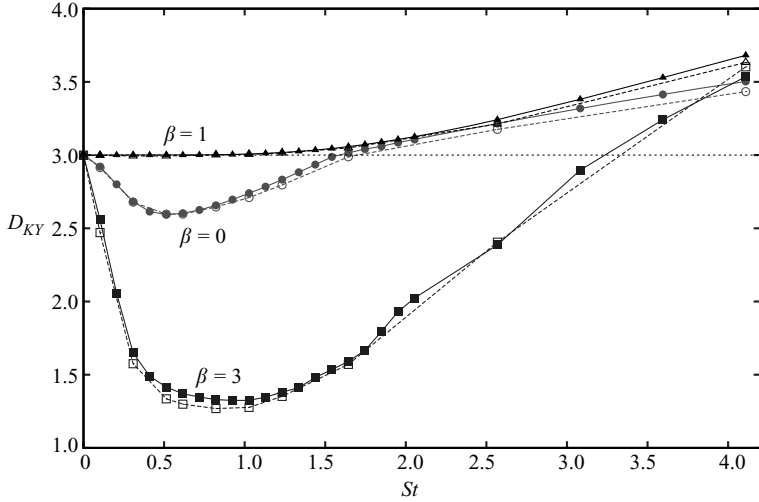
FIGURE 3. The Kaplan–Yorke dimension D_{KY} vs. St for three β values: $\beta = 0$ ($\circ$), 1 ($\triangle$), 3 ($\square$). Results at two different Re_λ are reported: $Re_\lambda = 75$ (filled symbols), $Re_\lambda = 180$ (open symbols).
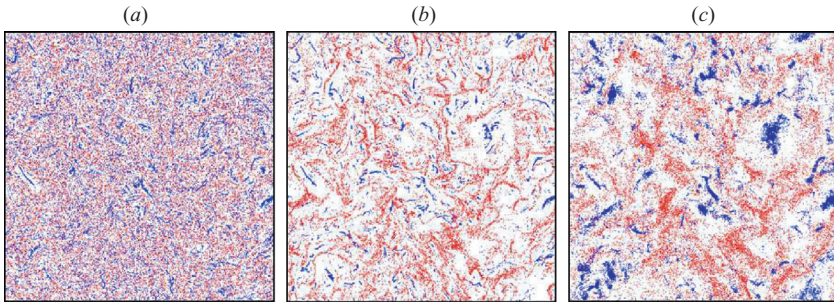

FIGURE 4. Projection of the particles in a slice of 19η thickness and side $640\eta \times 640\eta$ with $Re_\lambda = 180$, for (a) $St = 0.1$, (b) $St = 0.6$, and (c) $St = 4$. Heavy particles ($\beta = 0$) are shown in red, bubbles ($\beta = 3$) in blue. To illustrate the different clustering, particles and bubbles in the same simulation are plotted on top of each other – note that they do not mutually interact, i.e. collisions and feedback on the fluid are neglected.

shown for both $Re_\lambda = 75$ and $Re_\lambda = 180$, revealing at most a minute Reynolds number dependence of D_{KY}.

We now discuss the dependence $D_{KY}(\beta, St)$: point particles ($St = 0$, $\beta = 1$) do not experience any drag ($\boldsymbol{v} = \boldsymbol{u}$) and accordingly $D_{KY} = 3$. For fixed β the contraction is strongest for a Stokes parameter St in the range between 0.5 and 1.5, i.e. when the characteristic time scale τ_p of the particle roughly agrees with the Kolmogorov time scale τ_η. For smaller St the particles follow the small-scale turbulent fluctuations and the clustering decreases and D_{KY} increases. For large St the particles are so big that they average out the small-scale turbulent fluctuations (see figure 4); correspondingly, the clustering decreases and D_{KY} increases. The dynamical evolution of the heavy particles ($\beta = 0$) shows the strongest contraction for $St \approx 0.5$ with $D_{KY} = 2.6$. Also, that of the light particles ($\beta = 3$) has the strongest contraction for $St \approx 0.5$, and $D_{KY} = 1.4$ is achieved. Figures 2 and in 3 reveal another feature of D_{KY} which is worth noting: $D_{KY}(St, \beta = 1)$ slightly increases with increasing St, reflecting the fact
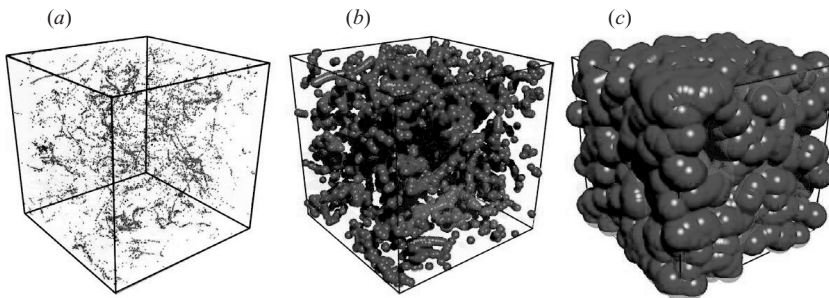
FIGURE 5. Visualization of $\mathscr{A}_r$: $N = 10^4$ point-like bubbles ($\beta = 3$, $St = 1$) in the turbulent flow are enclosed with in spheres of radius r, with (*a*) $r = 0.625\eta$, (*b*) $r = 3.75\eta$, and (*c*) $r = 12.5\eta$, respectively.

that large particles, even if neutrally buoyant, do not exactly follow the flow, see the discussion in Babiano *et al.* (2000).

An analysis of the spatial distribution performed with the correlation dimension D_2 (Grassberger & Procaccia 1984) yields very similar results as that for D_{KY}, see figure 2(*b*) (see also Bec, Cencini & Hillerbrand 2007 for further details on this observable). D_2 is computed by fitting the separation probability $P_2(r)$, which is the probability that the distance between two particles is less than r. It is assumed that $P_2(r) \sim r^{D_2}$ as $r \rightarrow 0$. As numerical convergence is more difficult to achieve for D_2, the curve $D_2(\beta, St)$ is slightly less smooth compared to $D_{KY}(\beta, St)$. The finiteness of the particle samples, here roughly 20 snapshots of 10^5 particles, leads to noisy measures especially for the highly clustered cases ($\beta \sim 3$): point particles may reach vanishingly small distances apart which makes it difficult to perform a proper histogram binning, and thus to compute statistically stable $P_2(r)$.

Owing to its local character a metric measurement with the Kaplan–Yorke or correlation dimension cannot supply us with global morphological information. Indeed, as seen from figure 2, clusters of heavy and light particles can have the same D_{KY}, though they look very different: the striking morphological differences of the particle and bubble distribution within the same turbulent velocity field are illustrated in figure 4.

3. Morphology of particle and bubble clusters

With global geometrical and topological order parameters we are able to distinguish the clustering on spatially extended, eventually interconnected, sheets from clouds or filamentary clustering. Consider the union set $\mathscr{A}_r = \bigcup_{i=0}^{N} \mathscr{B}_r(\boldsymbol{x}_i)$ of spheres of radius r around the N particles at positions $\boldsymbol{x}_i$, $i = 1, 2, \ldots N$, thereby creating connections between neighbouring spheres; see figure 5 for a visualization of $\mathscr{A}_r$ for three different sphere radii r. The global morphology of the union set of these spheres changes with radius r, which is employed as a diagnostic parameter. It seems sensible to request that global geometrical and topological measures of e.g. $\mathscr{A}_r$ are additive, invariant under rotations and translations, and satisfy a certain continuity requirement. With these prerequisites Hadwiger (1957) proved that in three dimensions the four Minkowski functionals $V_\mu(r)$, $\mu = 0, 1, 2, 3$, give a complete morphological characterization of the body $\mathscr{A}_r$. The Minkowski functional $V_0(r)$ is simply the volume of $\mathscr{A}_r$, $V_1(r)$ is a sixth of its surface area, $V_2(r)$ is its mean curvature divided by 3π, and $V_3(r)$ is its Euler characteristics. Volume and surface area are well-known quantities. The integral mean curvature and the Euler characteristic

are defined as surface integrals over the mean and the Gaussian curvature respectively. This definition is only applicable for bodies with smooth boundaries. In our case we have an additional contribution from the intersection lines and intersection points of the spheres. Mecke, Buchert & Wagner (1994) discuss the definitions of the integral mean curvature and the Euler characteristic for unions of convex bodies. The Euler characteristic as a topological invariant allows several other definitions, such as $\chi = \#(\text{isolated bodies}) - \#(\text{tunnels}) + \#(\text{completely enclosed cavities})$. Minkowski functionals have been developed for the morphological characterization of the large-scale distribution of galaxies by Mecke *et al.* (1994) and have successfully been used in cosmology by Kerscher *et al.* (1997), Kerscher (2000), Kerscher *et al.* (2001), porous and disordered media by Arns, Knackstedt & Mecke (2002), dewetting phenomena by Herminghaus *et al.* (1998), statistical physics in general (Mecke 2000) and have been recently employed to study magnetic structure in small-scale dynamos (Wilkin, Barenghi & Shukurov 2007).

There is an interesting relation to fractal dimensions. The scaling behaviour of the volume density for $r \to 0$ gives the Minkowski–Bouligand dimension of a fractal which equals the box-counting dimension, which is in turn an estimate of the Hausdorff dimension (see e.g. Falconer 1990). However owing to discreteness effects the scaling behaviour of the volume only yields a noisy estimate of the dimension. D_2 and D_{KY}, as used in our case, are much more reliable measures for the dimension. Since the Minkowski functionals are dimensional quantities, one is able to define other scaling dimensions beyond the volume. This has been formalized and investigated for special models by Mecke (2000). The open question remains of how to apply this to points enclosed with in spheres.

In figure 6 we show the volume densities of the four Minkowski functionals $v_\mu(r) = V_\mu(r)/L^3$, $\mu = 0, 1, 2, 3$, determined from the particle distributions with $St = 0.6$ for the three cases with $\beta = 3$ (bubbles), $\beta = 0$ (heavy particles), and $\beta = 1$ (neutral tracers). For the neutral tracers ($\beta = 1$) the functionals coincide with the analytically known values (Mecke & Wagner 1991) for randomly distributed objects. As the radius increases, the volume is filled until reaching complete coverage where the volume density $v_0(r)$, i.e. the filling factor, reaches unity. This increase is considerably delayed for heavy particles and even more for bubbles, which is a characteristic feature of a clustering distribution produced from the empty space between the clusters.

The density of the surface area, measured by $v_1(r)$, increases with the radius r. As more and more spheres overlap the growth of $v_1(r)$ slows down and the surface area reaches a maximum. For large radii the spheres fill the volume and no free surface area is left. For both the bubbles and the heavy particles the maximum of $v_1(r)$ is smaller compared to the Poisson case. For intermediate and large radii we observe the skewed shape of $v_1(r)$ with a significant excess of surface area on large scales compared to the Poisson case. The particles cluster on clumpy, filamentary and sheet-like structures and the surface area of the spheres is growing into the empty space between. Especially for the bubbles ($\beta = 3$) the maximum of $v_1(r)$ is attained for considerably larger r compared to the distributions with $\beta = 0, 1$, suggesting mainly separated filamentary shaped clusters.

The density of the integral mean curvature $v_2(r)$ allows us to differentiate convex from concave situations. For small radii the spheres are growing outward. The main contribution to the integral mean curvature is positive, coming from the convex parts. Increasing the radius further we observe a maximum for all three cases, but as with the surface area, the amplitude of the maximum is reduced for heavy particles and especially for the bubbles. For tracer particles ($\beta = 1$) the empty holes start
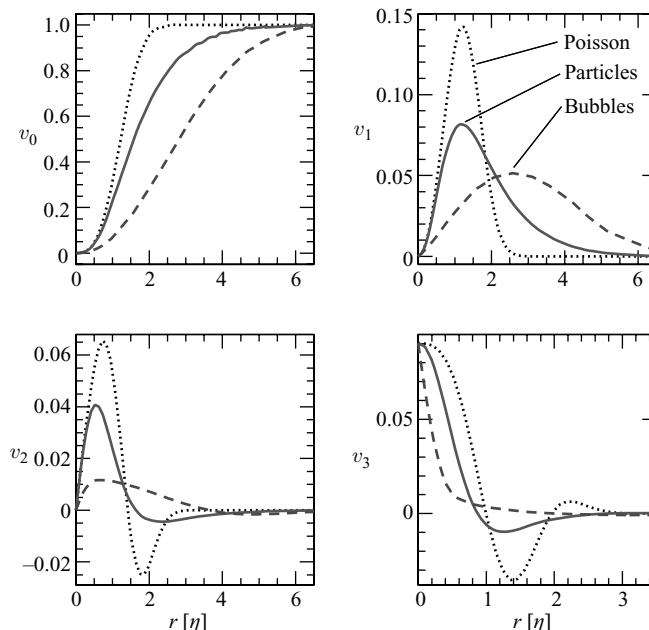
FIGURE 6. Volume densities of the Minkowski functionals $v_\mu(r)$, $\mu = 0, 1, 2, 3$, for passive tracers ($\beta = 1$, dotted, corresponding to those of a Poisson distribution (Mecke & Wagner 1991)), heavy particles ($\beta = 0$, solid), and bubbles ($\beta = 3$, dashed). In all cases $St = 0.6$ and $Re_\lambda = 78$. Distances are in Kolmogorov units (η). To estimated the errors in the Minkowski functionals we looked at several realizations of a Poisson process. The one sigma error bars are smaller than the thickness of the curves shown which illustrates the robustness of the Minkowski functionals. The code used for the calculations of the Minkowski functionals is an updated version of the code developed by Kerscher *et al.* (1997), based on the methods outlined in Mecke *et al.* (1994). The code is made available to the general public via http://www.mathematik.uni-muenchen.de/~kerscher/software/.

to fill and the structure is growing into the cavities. Now the main contribution to the integral mean curvature is negative, stemming from the holes and tunnels through the structure. This concaveness is less pronounced for the heavy particle case ($\beta = 0$). Typically, interconnected networks of tunnels show such a reduced negative contribution. For bubbles ($\beta = 3$) $\mathscr{A}_r$ is only just concave, i.e. no holes and no tunnels develop, just as expected from isolated (filamentary) clusters. For large radii the spheres fill the volume, and no free surface and hence no curvature is left.

The topology undergoes a number of changes which we measure with the Euler characteristic. For small radii $r \approx 0$ the spheres remain separated and the volume density of the Euler characteristic $v_3(r \approx 0)$ equals the number density of the particles. As the radius increases, spheres join up and the Euler characteristic decreases. Both for heavy particles ($\beta = 0$) and especially for bubbles ($\beta = 3$) the decrease of $v_3(r)$ with increasing r is more dramatic, because of the clustering. When further increasing the radius r, more and more tunnels start to form resulting in a negative $v_3(r)$. This is observed for neutral particles ($\beta = 1$) and is less pronounced for the heavy particles ($\beta = 0$). No tunnels seem to form in the bubble distribution ($\beta = 3$). For neutral particles this behaviour reaches a turning point when these tunnels are blocked to form closed cavities and a second positive maximum of $v_3(r)$ can be seen. Neither bubbles nor heavy particles show a significant positive $v_3(r)$.

To develop a physical picture we first look at the heavy particles. One expects that the particles are dragged out of the turbulent vortices, collecting on structures around the vortices. A dimension $D_{KY} \approx 2.6$ indicates 'fat' locally two-dimensional structures. From the negative $v_2(r)$ for large r we conclude that these two-dimensional structures are mainly concave, i.e. growing inward. Hence these two-dimensional structures are not small two-dimensional patches, but enclose the vortices. The particles around the vortices form the enclosure of tunnels but they do not fully enclose the vortices (they do not form the 'casing of a sausage'). Completely enclosed cavities would lead to a $v_3(r)$ larger zero for large r, which we do not observe. There must be regions connecting the vortices devoid of any particles. In other words there exists an empty interconnected network of tunnels surrounded by particles.

For the bubble distribution one expects that the bubbles are sucked into the vortices. The dimensional analysis with $D_{KY} \approx 1.4$ now suggests 'fat' locally one-dimensional structures. For the bubble distribution $v_2(r)$ is almost everywhere positive, hence the one-dimensional structures remain convex for all radii. Similarly $v_3(r)$ is positive on all scales. Hence, neither tunnels devoid of bubbles nor empty cavities enclosed by bubbles form. The one-dimensional structures built from the bubbles are separated filamentary clusters. This also shows that the bubbles do not form a structure percolating throughout the simulation.

Minkowski functionals calculated from points decorated with spheres depend on the number density of the point distribution. One can derive explicit expression in terms of high-order correlation functions quantifying the non-trivial dependence on the number density (see e.g. Mecke 2000). In our analysis we always compare data sets with the same number of points. However one may ask how well our Minkowski functionals are converged. In figure 7 the Minkowski functionals for a randomly subsampled data set are shown. Considering only 80 % of the points we obtain nearly a identical result as for the full sample. This can be understood as follows. We enclose the particles with in spheres. In our case the particles follow well-defined structures. For a radius equal to zero, v_3 equals the number density. That is why the v_3 curves fan out for small radii. For $r \approx 0.5\eta$ the curves for 100 %, 90 % and 80 % overlap again. In this sense our results are well converged.

Obviously, the convergence must be lost if we further reduce the number of points. Randomly subsampling (thinning) will inevitably lead to a convergence towards Poisson distribution (see the dotted line in figure 7) – the discreteness effects become more and more important.

Up to now we have investigated three extreme cases with $St = 0.6$ and $\beta = 0, 1, 3$. These three particle distributions also show different D_{KY}, hence their morphological differences do not come as a surprise. Now we investigate the morphology of particle distributions with similar D_{KY} but quite different physical parameters β and St. In figure 8 we compare heavy particles ($\beta = 0$, $St = 0.6$) with $D_{KY} = 2.59$ with light bubbles ($\beta = 3$, $St = 0.1$) with $D_{KY} = 2.55$. Clearly, their morphological properties differ. Although both have similar D_{KY}, the distribution of the heavy particle shows a stronger deviation from the Poisson distributed points than the light bubbles. As another example, in figure 8 we also compare the distribution of two sets of light bubbles, both with $\beta = 3$ and identical $D_{KY} = 1.65$, but with different Stokes number. The data set with $St = 1.75$ shows a distribution dominated by isolated clusters whereas the data set with $St = 0.4$ allows some interconnected empty tunnels.

We now address the Reynolds number dependence of the results from the morphological analysis. We compare the results for particles in turbulent flow with $Re_\lambda = 75$ with simulations at higher Reynolds numbers $Re_\lambda = 180$ and $Re_\lambda = 400$,
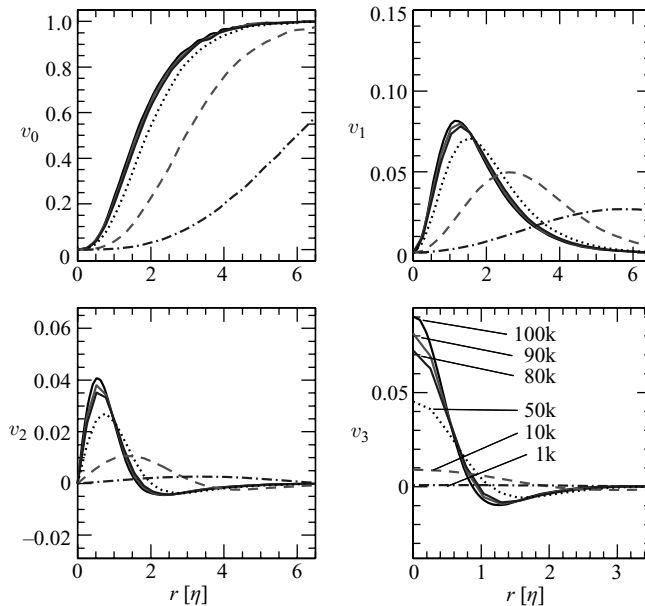
FIGURE 7. Volume densities of the Minkowski functionals $v_\mu(r)$, $\mu = 0, 1, 2, 3$ for the data set with $\beta = 0$ and $St = 0.6$. We compare the Minkowski functionals for samples with a different number of points, obtained by randomly thinning the original data set with 100k points: 100k points, 90k points, 80k points (all three solid, mostly on top of each other), 50k points (dotted), 10k points (dashed), 1k points (dashed–dotted).
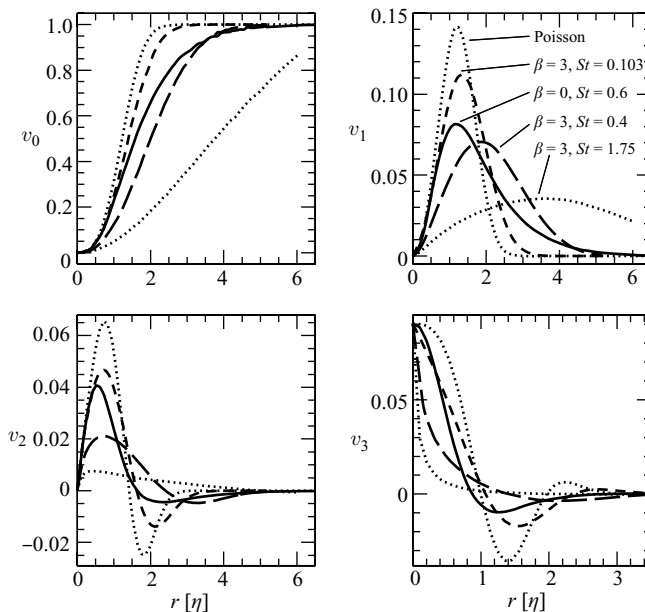

FIGURE 8. Volume densities of Minkowski functionals $v_\mu(r)$, $\mu = 0, 1, 2, 3$ for heavy particles with $\beta = 0$ and $St = 0.6$ (solid) and for light particles with $\beta = 3$ and $St = 0.1$ (short dashed): Whereas for these two particle types D_{KY} is basically the same, the Minkowski functionals clearly differ. As a second pair with nearly identical D_{KY} but different Minkowski functionals we compare two light particle distribution with differing Stokes parameter: $\beta = 3$, $St = 0.4$ (long dashed) to $\beta = 3$, $St = 1.75$ (dashed-dotted). Poisson distribution behaviour is reported for reference (dotted).
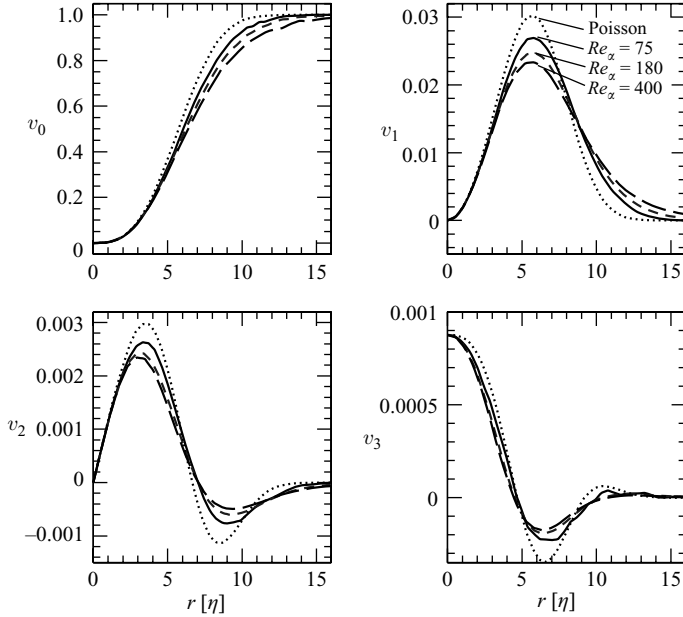
FIGURE 9. Volume densities of the Minkowski functionals $v_\mu(r)$, $\mu = 0, 1, 2, 3$ for particles with $\beta = 0$ and $St = 0.6$ in simulations with different Reynolds numbers: $Re_\lambda = 75$ (solid), $Re_\lambda = 180$ (short dashed), $Re_\lambda = 400$ (long dashed). Poisson distribution behaviour is reported for reference (dotted). All point sets have been subsampled to the same number density.

keeping the parameters $\beta = 0$ and $St = 0.6$ fixed. Only a weak dependence of the Minkowski functionals on the turbulence intensity can be seen in figure 9. A higher Reynolds number consistently corresponds to a slightly more pronounced deviation from the Poisson behaviour. We observe similar results for the bubble distribution with $\beta = 3$, $St = 0.6$. This result agrees with the very weak Reynolds dependence of D_{KY} already revealed in figure 3 and in Bec *et al.* (2006*a*).

4. Conclusions and outlook

The small-scale behaviour in a turbulent dispersed multiphase flow is often of interest. Then scaling or contraction indices like the Kaplan–Yorke dimension D_{KY} are the main investigation tools. With D_{KY} as a function of β and St a simple picture emerges: for heavy particles ($\beta < 1$) we observe in the extreme cases a scaling reminiscent of local planar structures; for light bubbles ($\beta > 1$) we find indications of local linear structures. The strength of the deviation from $D_{KY} = 3$ is further modulated by the Stokes parameter St. If one is interested in the connectivity and other (global) morphological features of the particle distribution, the picture becomes significantly more complex. The distribution of heavy particles seems to allow interconnected empty tunnels, whereas the distribution of bubbles typically shows isolated filamentary structures. But, depending on both β and St, interconnected structures also appear in the bubble distribution. Using Minkowski functionals as morphological order parameters we are able to quantify these geometrical and topological features in a unique way. In particular, we are able to overcome the degeneracy seen in D_{KY} as a function of β and St.

The next step is to use these tools to compare data obtained by particle tracking velocimetry (PTV) with those obtained from numerical simulations, in order to test

whether effective force models lead to the same particle distribution as measured in experiment. To facilitate such an analysis, we have made the code to calculate Minkowski functionals available to the general public, see http://www.mathematik.uni-muenchen.de/~kerscher/software/. Raw data can be downloaded from the International CFD database, iCFDdatabase (http://cfd.cineca.it).

REFERENCES

ARNS, C., KNACKSTEDT, M. & MECKE, K. 2002 Characterising the morphology of disordered materials. In *Morphology of Condensed Matter Physics and Geometry of Spatially Complex Systems* (ed. K. R. Mecke & D. Stoyan). Lecture Notes in Physics, vol. 600, pp. 37–74. Springer.

AYYALASOMAYAJULA, S., GYLFASON, A., COLLINS, L. R., BODENSCHATZ, E. & Z.WARHAFT 2006 Lagrangian measurements of inertial particle accelerations in grid generated wind tunnel turbulence. *Phys. Rev. Lett.* **97**, 144507.

BABIANO, A., CARTWRIGHT, J. H. E., PIRO, O. & PROVENZALE, A. 2000 Dynamics of a Small Neutrally Buoyant Sphere in a Fluid and Targeting in Hamiltonian Systems. *Phys. Rev. Lett.* **84**, 5764–5769.

BEC, J. 2003 Fractal clustering of inertial particles in random flows. *Phys. Fluids* **15**, L81–L84.

BEC, J. 2005 Multifractal concentrations of inertial particles in smooth random flows. *J. Fluid Mech.* **528**, 255–277.

BEC, J., BIFERALE, L., BOFETTA, G., LANOTTE, A. S., MUSACCHIO, S. & TOSCHI, F. 2006a Lyapunov exponents of heavy particles in turbulence. *Phys. Fluids* **18**, 091702.

BEC, J., BIFERALE, L., CENCINI, M., LANOTTE, A. S. & TOSCHI, F. 2006b Effects of vortex filaments on the velocity of tracers and heavy particles in turbulence. *Phys. Fluids* **18**, 081702.

BEC, J., CENCINI, M. & HILLERBRAND, R. 2007 Heavy particles in incompressible flows: The large stokes number asymptotics. *Physica* D **226**, 11–22.

VAN DEN BERG, T. H., LUTHER, S., MAZZITELLI, I., RENSEN, J., TOSCHI, F. & LOHSE, D. 2006 Bubbly turbulence. *J. Turb.* **7**, 1–12.

BEWLEY, G. P., LATHROP, D. P. & SREENIVASAN, K. R. 2006 Superfluid helium – visualization of quantized vortices. *Nature* **441**, 588.

BIFERALE, L., BOFFETTA, G., CELANI, A., LANOTTE, A. & TOSCHI, F. 2005 Particle trapping in three-dimensional fully developed turbulence. *Phys. Fluids* **17**, 021701.

BOIVIN, M., SIMONIN, O. & SQUIRES, K. 1998 Direct numerical simulation of turbulence modulation by particles in isotropic turbulence. *J. Fluid Mech.* **375**, 235–263.

BOURGOIN, M., OUELLETTE, N. T., XU, H. T., BERG, J. & BODENSCHATZ, E. 2006 The role of pair dispersion in turbulent flow. *Science* **311**, 835–838.

CALZAVARINI, E., VAN DEN BERG, T. H., TOSCHI, F. & LOHSE, D. 2008 Quantifying microbubble clustering in turbulent flow from single-point me asurements. *Phys. Fluids* **20**, 040702.

CALZAVARINI, E., CENCINI, M., LOHSE, D. & TOSCHI, F. 2007 Quantifying turbulence induced segregation of inertial particles. *Phys. Rev. Lett.* (submitted).

CELANI, A., FALKOVICH, G., MAZZINO, A. & SEMINARA, A. 2005 Droplet condensation in turbulent flows. *Europhys. Lett.* **70**, 775–781.

CHUN, J., KOCH, D. L., RANI, S. L., AHLUWALIA, A. & COLLINS, L. R. 2005 Clustering of aerosol particles in isotropic turbulence. *J. Fluid Mech.* **536**, 219–251.

CROWE, C. T., TROUTT, T. & CHUNG, J. N. 1996 Numerical models for two-phase turbulent flows. *Annu. Rev. Fluid Mech.* **28**, 11–43.

DRUZHININ, O. A. & ELGHOBASHI, S. 2001 Direct numerical simulation of a three-dimensional spatially developing bubble-laden mixing layer with two-way coupling. *J. Fluid Mech.* **429**, 23–61.

ECKMANN, J. P. & RUELLE, D. 1985 Ergodic theory of chaos and strange attractors. *Rev. Mod. Phys.* **67**, 617.

ELGHOBASHI, S. & TRUESDELL, G. 1992 Direct simulation of particle dispersion in a decaying isotropic turbulence. *J. Fluid Mech* **242**, 655–700.

ELGHOBASHI, S. & TRUESDELL, G. 1993 On the two-way interaction between homogeneous turbulence and dispersed solid particles. I: Turbulence modification. *Phys. Fluids* A **5**, 1790–1801.

FALCONER, K. J. 1990 *Fractal Geometry*. John Wiley & Sons.

FALKOVICH, G., FOUXON, A. & STEPANOV, M. G. 2002 Acceleration of rain initiation by cloud turbulence. *Nature* **419**, 151–154.

GATIGNOL, R. 1983 The Faxen formulae for a rigid particle in an unsteady non-uniform Stokes flow. *J. Méc. Théori. Appl.* **1**, 143–160.

GRASSBERGER, P. & PROCACCIA, I. 1984 Dimensions and entropies of strange attractors from a fluctuating dynamics approach. *Physica* D **13**, 34–54.

HADWIGER, H. 1957 *Vorlesungen über Inhalt, Oberfläche und Isoperimetrie*. Springer.

HERMINGHAUS, S., JACOBS, K., MECKE, K., BISCHOF, J., FERY, A., IBN-ELHAJ, M. & SCHLAGOWSKI, S. 1998 Spinodal dewetting in liquid crystal and liquid metal films. *Science* **282**, 916–919.

HOYER, K., HOLZNER, M., LUETHI, B., GUALA, M., LIEBERZON, A. & KINZELBACK, W. 2005 3D scanning particle tracking velocimetry. *Exps. Fluids* **39**, 923–934.

KERSCHER, M. 2000 Statistical analysis of large–scale structure in the Universe. In *Statistical Physics and Spatial Statistics: The Art of Analyzing and Modeling Spatial Structures and Pattern Formation* (ed. K. R. Mecke & D. Stoyan). Lecture Notes in Physics, vol. 554. Springer.

KERSCHER, M., MECKE, K., SCHMALZING, J., BEISBART, C., BUCHERT, T. & WAGNER, H. 2001 Morphological fluctuations of large–scale structure: the PSCz survey. *Astron. Astrophys.* **373**, 1–11.

KERSCHER, M., SCHMALZING, J., RETZLAFF, J., BORGANI, S., BUCHERT, T., GOTTLÖBER, S., MÜLLER, V., PLIONIS, M. & WAGNER, H. 1997 Minkowski functionals of Abell/ACO clusters. *Mon. Not. R. Astron. Soc.* **284**, 73–84.

MALKIEL, E., ABRAS, J. N., WIDDER, E. A. & KATZ, J. 2006 On the spatial distribution and nearest neighbor distance between particles in the water column determined from in situ holographic measurements. *J. Plankton Res.* **28**, 149–170.

MARCHIOLI, C. & SOLDATI, A. 2002 Mechanisms for particle transfer and segregation in a turbulent boundary layer. *J. Fluid Mech.* **468**, 283–315.

MAXEY, M. & RILEY, J. 1983 Equation of motion for a small rigid sphere in a nonuniform flow. *Phys. Fluids* **26**, 883–889.

MAZZITELLI, I., LOHSE, D. & TOSCHI, F. 2003a The effect of microbubbles on developed turbulence. *Phys. Fluids* **15**, L5–L8.

MAZZITELLI, I., LOHSE, D. & TOSCHI, F. 2003b On the relevance of the lift force in bubbly turbulence. *J. Fluid Mech.* **488**, 283–313.

MECKE, K. 2000 Additivity, convexity, and beyond: Application of minkowski functionals in statistical physics. In *Statistical Physics and Spatial Statistics: The Art of Analyzing and Modeling Spatial structures and Pattern Formation* (ed. K. Mecke & D. Stoyan). Lecture Notes in Physics, vol. 554. Springer.

MECKE, K. R., BUCHERT, T. & WAGNER, H. 1994 Robust morphological measures for large–scale structure in the Universe. *Astron. Astrophys.* **288**, 697–704.

MECKE, K. R. & WAGNER, H. 1991 Euler characteristic and related measures for random geometric sets. *J. Statist. Phys.* **64**, 843–850.

PORTA, A. L., VOTH, G. A., CRAWFORD, A. M., ALEXANDER, J. & BODENSCHATZ, E. 2001 Fluid particle accelerations in fully developed turbulence. *Nature* **409**, 1017–1019.

UPSTILL-GODDARD, R. C. 2006 Air-sea gas exchange in the coastal zone. *Esturine Coastal Shelf Sci.* **70**, 388–404.

VAILLANCOURT, P. A., YAU, M. K., BARTELLO, P. & GRABOWSKI, W. W. 2002 Microscopic approach to cloud droplet growth by condensation. part ii: Turbulence, clustering, and condensational growth. *J. Atmos. Sci.* **59**, 3421–3435.

WANG, L. & MAXEY, M. 1993 Settling velocity and concentration distribution of heavy particles in homogeneous isotropic turbulence. *J. Fluid Mech.* **256**, 27–68.

WILKIN, S. L., BARENGHI, C. F. & SHUKUROV A. 2007 Magnetic structures produced by the small-scale dynamo. *Phys. Rev. Lett.* **99**, 134301.